Catalysis Today 164 (2011) 198–203

Contents lists available at ScienceDirect

Catalysis Today

journal homepage: www.elsevier.com/locate/cattod

High temperature adsorption of CO_2 on Mg–Al hydrotalcite: Effect of the charge compensating anions and the synthesis pH

Qiang Wang[a], Zhihuai Wu[a,b], Hui Huang Tay[a], Luwei Chen[a], Yan Liu[a], Jie Chang[a], Ziyi Zhong[a], Jizhong Luo[a,*], Armando Borgna[a]

[a] Applied Catalysis, Institute of Chemical and Engineering Sciences (ICES), A*STAR, 1 Pesek Road, Jurong Island, 627833 Singapore, Singapore
[b] School of Materials Science and Engineering, Nanyang Technological University (NTU), 50 Nanyang Avenue, 639798 Singapore, Singapore

ARTICLE INFO

Article history:
Available online 11 November 2010

Keywords:
CO_2 capture
Sorption enhanced water gas shift
Layered double hydroxide
Anion effect
Global warming

ABSTRACT

This work reported a detailed investigation on how charge compensating anions and synthesis pH affect the structural properties and CO_2 adsorption capacity of Mg–Al hydrotalcites (HTs). A series of Mg_3Al_1–A (A = CO_3^{2-}, HCO_3^-, NO_3^-, SO_4^{2-}, and Cl^-) HTs were synthesized and tested as high temperature CO_2 adsorbents. It was found that the anions have great effect on the thermal stability and morphology, as well as on the surface area of HTs, consequently influencing the CO_2 adsorption capacity of HT derivatives. Among various HTs, Mg_3Al_1–CO_3 showed the highest CO_2 adsorption capacity of 0.53 mmol/g. Next, the influence of synthesis pH on the Mg/Al ratio, BET surface area, pore size, and CO_2 adsorption capacity of Mg_3Al_1–CO_3 was investigated. Mg_3Al_1–CO_3 synthesized at pH = 10–12 showed good performance for CO_2 adsorption. By doping Mg_3Al_1–CO_3 (pH = 10) with 20 wt.% K_2CO_3, the CO_2 adsorption capacity was increased up to 0.85 mmol/g.

1. Introduction

Sorption-enhanced water gas shift (SEWGS) is being widely regarded as a promising pre-combustion CO_2 capture technology. This process is a combination of WGS reaction and CO_2 adsorption, as shown in reaction (1) [1–3].

$$CO(g) + H_2O(g) + \text{adsorbent}(s) \leftrightarrow \text{adsorbent}{-}CO_2(s) + H_2(g) \quad (1)$$

By adsorbing and removing CO_2 from the reaction mixture, the reaction is driven to the right-hand-side, thereby completely converting CO and maximizing the production of H_2. SEWGS produces a hot stream of hydrogen and steam which can be directly fed to a gas turbine and a cooled stream of pure CO_2 which can be compressed and transported for further storage and utilization. To ensure the success of this technology, it is crucial to have good CO_2 adsorption materials, which should be able to stand with ten thousands to a hundred thousand of sorption and regeneration operations. When the sorbent is saturated with CO_2, it should be regenerated and re-used. Generally speaking, the sorbent materials should possess a sufficiently high and reversible CO_2 adsorption capacity, a fast adsorption and desorption kinetics, and good mechanical/thermal stability in the temperature range of 200–500 °C and in the pressure range of 1–40 bar [4–7].

Among various CO_2 adsorbents, hydrotalcite-based materials (HTs) have been identified as suitable materials for high temperature (200–400 °C) adsorption of CO_2 [8–10]. Fresh HT itself does not possess any basic sites. Upon thermal treatment, HT gradually loses interlayer water, and then dehydroxylates and decarbonates to a large extent, leading to the formation of a mixed oxide with 3D network [11]. Ram Reddy et al. [12] investigated the calcination temperature effect on the CO_2 adsorption capacity of Mg–Al–CO_3 HT. The sample calcined at 400 °C showed the highest adsorption capacity, which could be due to the tradeoff between the surface area and availability of active basic sites. This amorphous phase has a relatively high surface area and exposes sufficient basic sites on the surface. These basic sites favor reversible CO_2 adsorption in the form shown in Eq. (2) [13]. The interaction between the adsorbed CO_2 and the basic sites is stronger than that with zeolite, but weaker than that with alkali metal oxide, implying a potential of using HT derivatives as high temperature CO_2 adsorbents (>200 °C) [12–15].

$$Mg{-}O + CO_2 \rightarrow Mg{-}O{\cdots\cdots}CO_2(ad) \quad (2)$$

For further developments and improvements of high temperature CO_2 adsorbents, a lot of work has been done on HTs, especially on the modification of Mg–Al–CO_3 [16–19]. Recently, our group reported the effect of trivalent cations on the performance of Mg–M^{3+}–CO_3 (M^{3+} = Al^{3+}, Fe^{3+}, Ga^{3+}, Mn^{3+}, etc.) HTs for high-temperature CO_2 capture, clearly showing that the M^{3+} cations determine the structure evolution of HT derivatives under thermal treatment, which finally influences the CO_2 capture capacity. It was also found that the quasi-amorphous phase obtained by ther-

* Corresponding author. Tel.: +65 6796 3830; fax: +65 6316 6182.
E-mail addresses: wang_qiang@ices.a-star.edu.sg (Q. Wang), luo_jizhong@ices.a-star.edu.sg (J. Luo).

0920-5861/$ – see front matter © 2010 Elsevier B.V. All rights reserved.
doi:10.1016/j.cattod.2010.10.042

mal treatment at the lowest possible temperature gave the highest CO_2 capture capacity [20]. However, there are still several problems that remain unsolved for HT adsorbents, for instance the effect of charge compensating anions as well as the effect of synthesis pH. In this contribution, a series of Mg_3Al_1–A (A = CO_3^{2-}, NO_3^-, Cl^-, SO_4^{2-}, and HCO_3^-) HTs were synthesized and investigated as high temperature CO_2 adsorbents. The influence of the synthesis pH on the chemical composition and CO_2 adsorption capacity of Mg_3Al_1–CO_3 was also studied in detail. Finally, the promotion effect of K_2CO_3 on CO_2 capture was evaluated by doping Mg_3Al_1–CO_3 (pH = 10) with 20 wt.% K_2CO_3.

2. Experimental

2.1. Preparation of HTs and K_2CO_3/HTs

HTs with Mg/Al = 3 were synthesized using a co-precipitation method. All chemicals were purchased from Merck KGaA (Germany) and Sigma–Aldrich (USA). Mg_3Al_1–CO_3, Mg_3Al_1–NO_3, and Mg_3Al_1–SO_4 were synthesized by adding a $Mg(NO_3)_2{\cdot}6H_2O$ and $Al(NO_3)_3{\cdot}9H_2O$ solution drop-wise into a Na_2CO_3, or $NaNO_3$, or Na_2SO_4 solution, respectively. The pH of the precipitation was controlled at ~10 using a NaOH solution. Mg_3Al_1–Cl was prepared by adding a $MgCl_2$ and $AlCl_3{\cdot}xH_2O$ solution into a NaCl solution, with the pH controlled at ~10 using a NaOH solution. Mg_3Al_1–HCO_3 was synthesized by dropping a $Mg(NO_3)_2{\cdot}6H_2O$ and $Al(NO_3)_3{\cdot}9H_2O$ solution into a $NaHCO_3$ solution. The pH of the precipitation solution was strictly controlled at ~8.5 using a NaOH solution, as any decrease in the pH will cause HCO_3^- to decompose into CO_2, and any increase in the pH will transform HCO_3^- into CO_3^{2-}. For all the above syntheses, 50 ml Mg–Al precursor solution containing 0.0375 mol Mg^{2+} and 0.0125 mol Al^{3+}, and 50 ml anion precursor solution containing 0.025 mol anions were used. The NaOH solution was 3.4 M. The pH values were measured using a pH Benchtop meter (Orion 2 star, Thermo Scientific). Mg_3Al_1–CO_3 HTs were also synthesized at different pH values, ranging from 6.5 to 14.

K_2CO_3/HT was prepared according to the following procedure: HT was first pretreated at 400 °C in Ar flow for 5 h. Next, the calcined HT, 20 wt.% K_2CO_3, and small amount of H_2O were completely mixed by ball milling for 10 h at 250 rpm. The mixture was then re-calcined at 400 °C in Ar flow for 5 h to give K_2CO_3/HT.

2.2. Characterization of HTs and K_2CO_3/HTs

The BET (Brunauer, Emmet, and Teller) specific surface areas were measured from the N_2 adsorption and desorption isotherms at 77 K collected from a Quantachrome Autosorb-6B surface area and pore size analyzer. Powder X-ray diffraction (XRD) analyses were conducted on a Bruker D8 Advance X-ray diffractometer equipped with a RINT 2000 wide-angle goniometer using Cu Kα radiation and a power of 40 kV × 40 mA. Diffraction patterns were recorded within the range of 2θ = 5–70° with a step size of 0.02°. During thermal treatment of HTs, the weight loss was determined using a thermal gravimetric analyzer (TGA Q500, TA Instruments). The sample was heated in N_2 from 30 to 600 °C with a ramping rate of 5 °C/min. The morphologies of samples were characterized by scanning electron microscope (SEM, JEOL JSM-6700F). Fourier transform infrared spectrometer (FT-IR) experiments were performed using a FTS 3000 MX FT-IR spectrophotometer. The elemental composition of synthesized HTs was analyzed by inductively coupled plasma-optical emission spectrometer (ICP-OES, Varian Vista-MPX CCD Simultaneous ICP-OES) after the samples were digested using aqua regia and kept in 2% HNO_3.

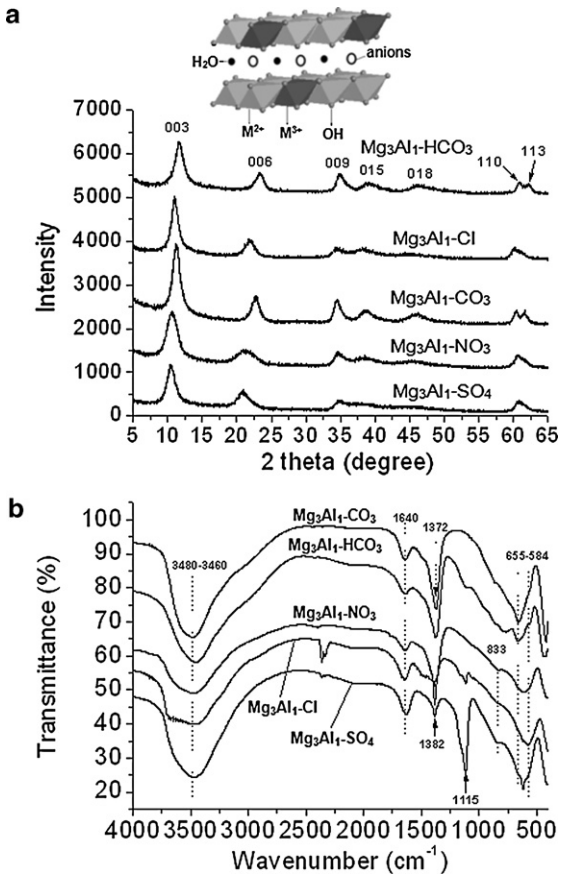

Fig. 1. (a) XRD patterns of synthesized Mg_3Al_1–SO_4, Mg_3Al_1–NO_3, Mg_3Al_1–CO_3, Mg_3Al_1–Cl, and Mg_3Al_1–HCO_3. The inset shows the schematic structure of HTs. (b) FTIR analyses of synthesized Mg_3Al_1–CO_3, Mg_3Al_1–HCO_3, Mg_3Al_1–NO_3, Mg_3Al_1–Cl, and Mg_3Al_1–SO_4.

2.3. Measurement of CO_2 capture capacity

Thermogravimetric sorptions of CO_2 on HTs and K_2CO_3/HTs were measured using a Q500 TGA analyzer. Samples were first calcined at 400 °C for 5 h in Ar atmosphere in a tube furnace before being transferred into TGA analyzer. To minimize the error caused by memory effect, all experiments were carried out immediately after the first calcination, and the samples were further calcined in situ at 400 °C for 1 h in N_2 before adsorption. CO_2 adsorption experiments were carried out at 1 atm with a constant flow of CO_2 (20 ml/min).

3. Results and discussion

3.1. Effect of charge compensating anions

XRD analysis was first utilized to study the formation of synthesized Mg_3Al_1–CO_3, Mg_3Al_1–NO_3, Mg_3Al_1–SO_4, Mg_3Al_1–Cl, and Mg_3Al_1–HCO_3. The XRD patterns are shown in Fig. 1(a). It is apparent that all five HTs have formed typical layered double hydroxide structure. A slight difference in the interlayer distance was observed when various anions were used, probably due to their difference in dimension and carried charges. When CO_3^{2-} was inserted as a guest anion, the interlayer distance was ~7.80 Å; while when SO_4^{2-} was inserted, the distance was expanded to 8.85 Å. The basal spacing values (d_{003}) for all five HTs are summarized in Table 1. The inset of Fig. 1(a) shows the schematic structure of HTs, in which the interlayer anions are highly exchangeable. In the present work, we are interested in how these anions influence the

Table 1
Basal spacing d_{003}, BET surface area, CO_2 capture capacity, and molecular formula of synthesized Mg_3Al_1–CO_3, Mg_3Al_1–NO_3, Mg_3Al_1–SO_4, Mg_3Al_1–Cl, and Mg_3Al_1–HCO_3.

HTs	d_{003} (nm)	BET, before calcination, (m^2/g)	BET, after calcination, (m^2/g)	CO_2 capture capacity (mmol/g)	Molecular formula
Mg_3Al_1–CO_3	7.80	114.3	239.0	0.53	$Mg_3Al_1(OH)_8(CO_3)_{0.5}\cdot 2H_2O$
Mg_3Al_1–NO_3	8.80	8.1	114.9	0.21	$Mg_3Al_1(OH)_8NO_3\cdot 2H_2O$
Mg_3Al_1–SO_4	8.85	5.2	41.9	0.10	$Mg_3Al_1(OH)_8(SO_4)_{0.5}\cdot 2H_2O$
Mg_3Al_1–Cl	8.04	4.9	136.5	0.18	$Mg_3Al_1(OH)_8Cl\cdot 2H_2O$
Mg_3Al_1–HCO_3	7.85	5.9	135.6	0.18	$Mg_3Al_1(OH)_8HCO_3\cdot 2H_2O$

CO_2 adsorption capacity of HTs.To ensure that we have successfully synthesized the HTs with aimed anions, FTIR analysis was also performed. The results are shown in Fig. 1(b). The characteristic peaks of HTs were observed for all synthesized samples. The –OH stretch in the brucite-like layer appeared at around 3460–3480 cm^{-1}; the vibration of angular deformation of H_2O molecules was seen at 1640 cm^{-1}; and the Al–O and Mg–O vibrations were found at 584–655 cm^{-1}. Interlayer anions slight influenced the peak positions of Al–O and Mg–O vibrations [21]. In addition, more information about the anions was obtained from the FTIR analysis. The peak at 1372 cm^{-1} for Mg_3Al_1–CO_3 and the peaks at 1382 cm^{-1} and 839 cm^{-1} for Mg_3Al_1–NO_3 were assigned to the vibrations of carbonate and nitrate respectively. For Mg_3Al_1–SO_4, the sulfate species was detected by the appearance of a peak at 1115 cm^{-1}; besides, a small peak at 1382 cm^{-1} suggested that certain amount of NO_3^- co-existed with SO_4^{2-} in the sample [22–23]. The frequency of bicarbonate vibration for Mg_3Al_1–HCO_3 was observed at around 1375 cm^{-1}. The peak at 2362 cm^{-1} for Mg_3Al_1–Cl was apparently due to the CO_2 background of the measurement system [24]. A rather weak peak at around 1384 cm^{-1} could correspond to either carbonate or nitrate group [25–26]. However, during the whole preparation process, there is no chance for Mg_3Al_1–Cl to contact with NO_x/nitrate. Therefore, this peak is most probably due to the carbonate anion which might have formed by the adsorption of atmospheric CO_2 [27–29]. Similar to the result reported by López et al. [21], the interlayer Cl^- bands cannot be observed in the studied region of the spectrum.

Their thermal stabilities were then investigated by TGA. Fig. 2(a) shows the TGA profiles of synthesized HTs, all of which are fairly similar in shape with two distinct regions of weight loss. The initial weight decrease of approximately 15% in the temperature range of 30–190 °C was due to the loss of loosely held water in the interlayer space [30]. And the second weight decrease in the temperature range of 250–500 °C was due to dehydroxylation of the octahedral layers as well as the decomposition of the interlayer anions. Mg_3Al_1–SO_4 showed a relatively higher thermal stability, and its second weight loss ends at around 480 °C; while for all other HTs, the second weight loss ends at around 400 °C. The total weight loss of all samples is around 38–47 wt.%.

Fig. 2(b) shows the XRD patterns of calcined HTs. After being calcined at 400 °C in Ar, all samples except Mg_3Al_1–SO_4 were transformed into amorphous mixed oxide, with periclase MgO as the main phase. For Mg_3Al_1–SO_4, a slightly higher calcination temperature (500 °C) was required to completely decompose its layered structure. This result is consistent with the TGA analysis and further confirmed that Mg_3Al_1–SO_4 has higher thermal stability. BET analysis was also performed on both fresh and calcined HTs, as shown in Table 1. For the first time, our result revealed that the interlayer anion is the key parameter that determines the BET surface area of HTs. The BET surface area of fresh Mg_3Al_1–CO_3 was very high, ~114.3 m^2/g; however, for other HTs with anions NO_3^-, Cl^-, SO_4^{2-}, and HCO_3^-, the BET surface areas became very low, <9 m^2/g. The morphology of synthesized HTs was investigated by SEM, as shown in Fig. 3. Mg_3Al_1–CO_3 formed spheroidal "sand rose" morphology (Fig. 3(a)). The size of "flower ball" was approximately 400–450 nm, and the thickness of petals was about 24–25 nm, which accounted for about 30–32 brucite-like sheets (Fig. 3(b)). The abundance of petal surface gave its high surface area. All other HTs formed "stone" morphology, with particle size ranged from several to several-tenth micro-meters. High-resolution SEM analysis indicated that these particles were nonporous (not shown here). Therefore, their surface areas were very low. The BET surface areas of HTs were greatly increased by thermal treatment at 400 °C in Ar (see Table 1). The BET of calcined Mg_3Al_1–CO_3 was 239 m^2/g, which was still much higher than other calcined samples (<140 m^2/g).

The CO_2 adsorption capacities of calcined Mg_3Al_1–A (A = CO_3^{2-}, SO_4^{2-}, NO_3^-, Cl^-, and HCO_3^-) HTs were then tested at 200 °C (see Table 1). Apparently, Mg_3Al_1–CO_3 showed the highest CO_2 adsorption capacity (0.53 mmol/g). This value was much higher than those for calcined Mg_3Al_1–SO_4, Mg_3Al_1–NO_3, Mg_3Al_1–Cl, and Mg_3Al_1–HCO_3 (~0.2 mmol/g). The results indicated that the BET surface area of calcined HTs seems be the main parameter that determines the CO_2 adsorption capacity. It was reported that the Mg–O which is exposed on the surface is the active basic site [12–15]. Because the surface area of calcined Mg_3Al_1–CO_3 (239 m^2/g) was much higher than those of the other calcined HTs, Mg_3Al_1–CO_3 derivative was supposed to provide more adsorp-

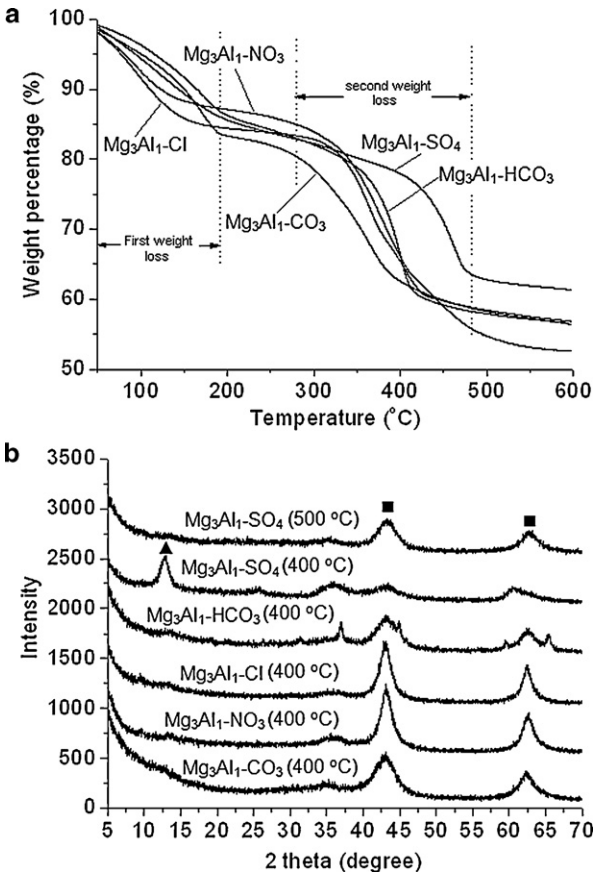

Fig. 2. (a) TGA analyses of synthesized Mg_3Al_1–CO_3, Mg_3Al_1–HCO_3, Mg_3Al_1–SO_4, Mg_3Al_1–NO_3, and Mg_3Al_1–Cl. (b) XRD patterns of calcined Mg_3Al_1–CO_3, Mg_3Al_1–NO_3, Mg_3Al_1–Cl, Mg_3Al_1–HCO_3, and Mg_3Al_1–SO_4 at 400 °C and 500 °C. (▲) HT, (■) periclase MgO.

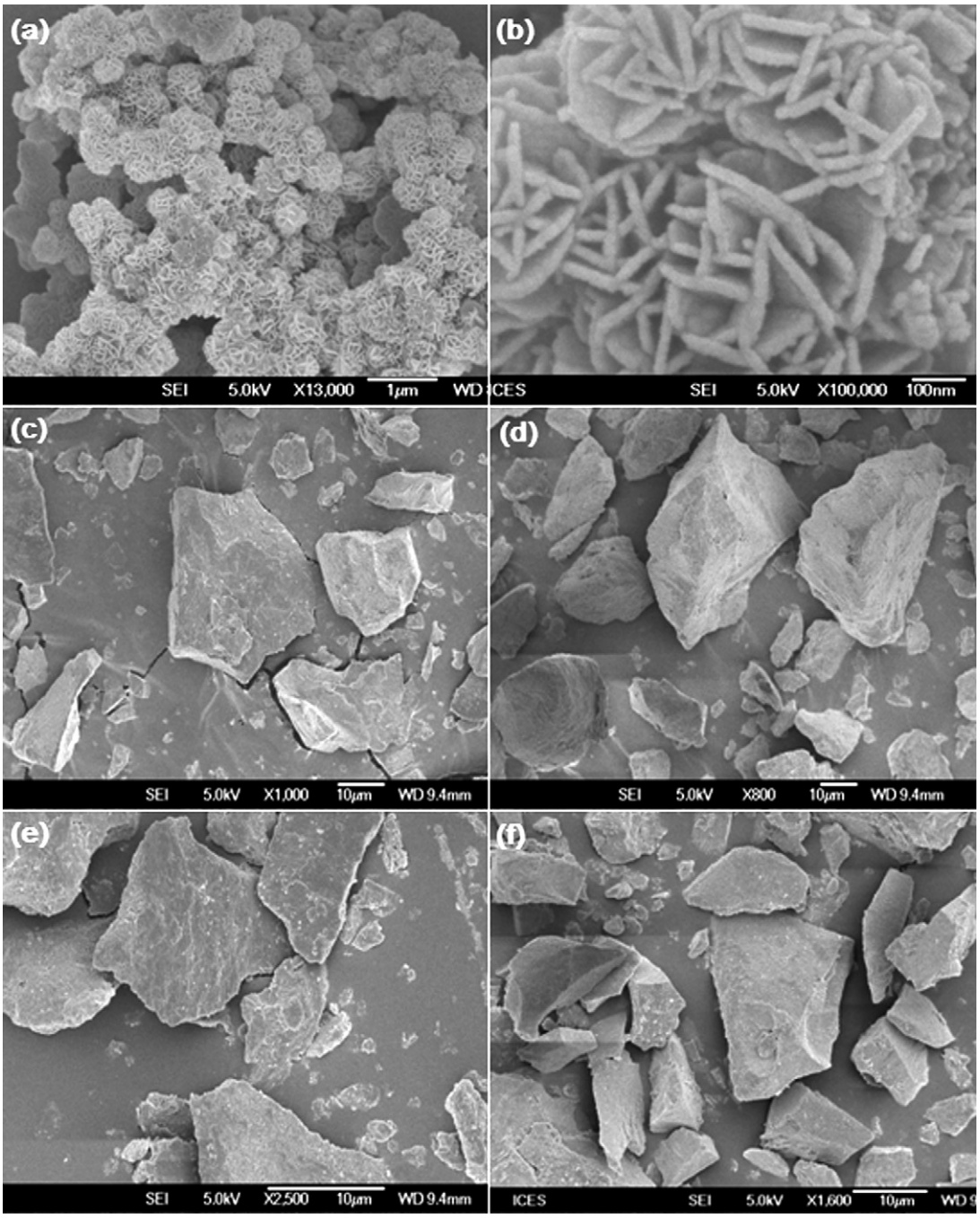

Fig. 3. SEM images of synthesized (a) Mg_3Al_1–CO_3, (b) Mg_3Al_1–CO_3 (high resolution), (c) Mg_3Al_1–NO_3, (d) Mg_3Al_1–SO_4, (e) Mg_3Al_1–Cl, and (f) Mg_3Al_1–HCO_3.

tion sites for CO_2. Besides, the morphology of the synthesized HTs might also affect CO_2 adsorption. The "sand rose" like HT possesses abundant of pores between "petals", and thus favors CO_2 diffusion as well as adsorption. However, "stone" like HTs was very big in size and nonporous. Last but not least, the thermal stability of HTs should also be considered for CO_2 capture. Although most of HTs have transformed into amorphous phase at 400 °C, certain anions cannot be completely decomposed at this temperature. And the remaining anions might occupy active adsorption sites. For instance, we observed that a calcination temperature as high as 500 °C was required to completely decompose NO_3^- into NO and O_2 from Mg_3Al_1–NO_3. However, if the calcination temperature is too high, the number of active Mg–O sites will decrease due to the formation of crystal MgO. Wang et al. [20] has demonstrated that the quasi-amorphous phase obtained by thermal treatment at the lowest possible temperature gave the highest CO_2 capture capacity. Therefore, it can be concluded that, because the anions have great effect on the thermal stability, morphology, as well as surface area of HTs, they have a significant influence on the CO_2 adsorption capacity of calcined HTs.

3.2. Effect of synthesis pH

Besides the effect of interlayer anions, CO_2 adsorption capacity is also affected by the synthesis conditions. In this work, the influence of synthesis pH on Mg_3Al_1–CO_3 was studied systematically. Fig. 4(a) shows the XRD patterns of synthesized Mg_3Al_1–CO_3 at pH 6.5–14. When pH is low (≤7), $Mg(OH)_2$ tends to dissociate into Mg^{2+} and

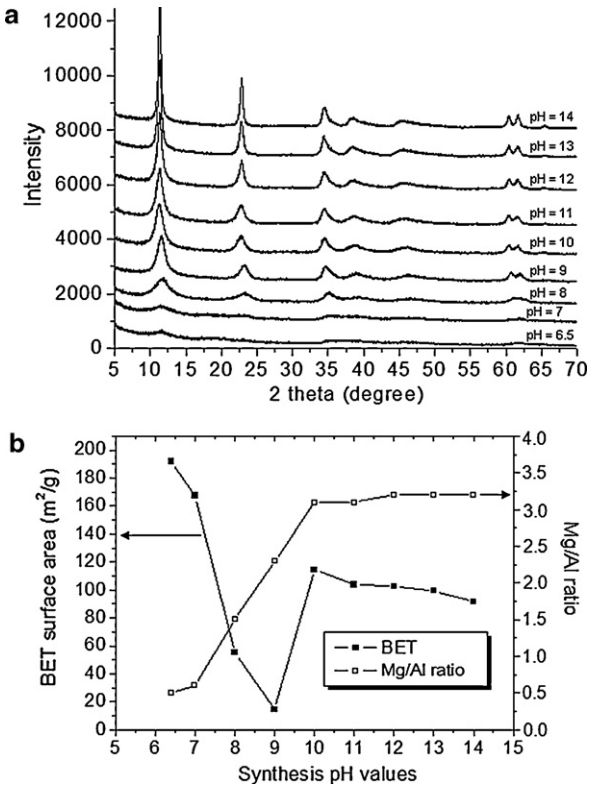

Fig. 4. (a) XRD patterns of Mg_3Al_1–CO_3 synthesized at various pH values. (b) BET surface area and the Mg/Al ratio of HTs as a function of synthesis pH.

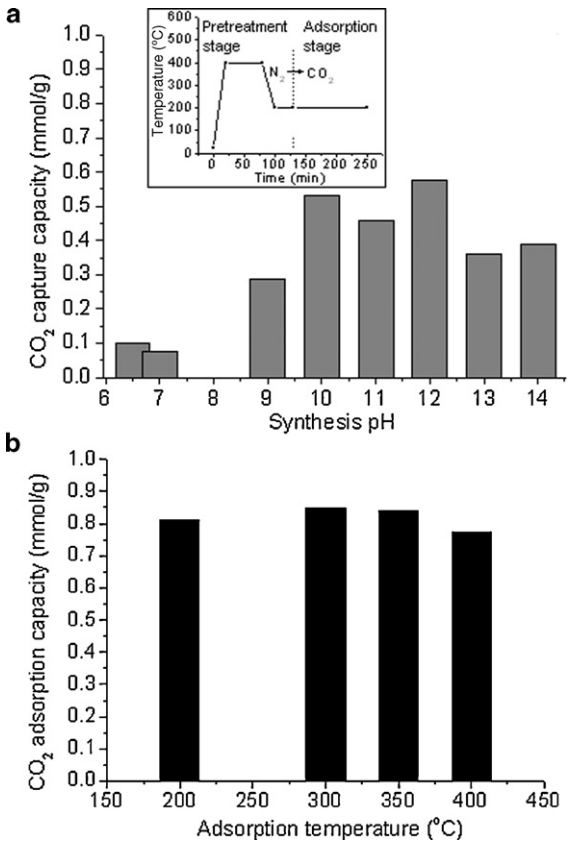

Fig. 5. (a) The influence of synthesis pH on the CO_2 adsorption capacity of Mg_3Al_1–CO_3 HTs (CO_2 adsorptions were tested at 200 °C). The inset shows the temperature profile for CO_2 adsorption test. (b) The influence of adsorption temperature on the CO_2 capture capacity of 20 wt.% K_2CO_3/Mg_3Al_1–CO_3 (pH = 10).

OH^- ions, and hence almost no HT structure was formed, resulting in an amorphous product which could be identified as AlOOH. With pH ≥ 8, the characteristic peaks of HT structure were clearly seen for all samples. In addition, the crystallinity degree of HTs formed increased with increasing pH values. ICP-OES analysis shown in Fig. 4(b) further confirmed the XRD result. When the synthesis pH was 6.5 or 7, the Mg/Al ratio was only 0.5–0.6, which is much lower than the theoretical value of 3. The Mg/Al ratio increased from 1.5 to 2.3 when the pH increased from 8 to 9, but it was still lower than the theoretical value of 3. Only samples with pH = 10 and above had the experimental ratio close to the theoretical ones. At high pH values (pH = 10–14), $Mg(OH)_2$ will first be formed and then immediately transformed into HTs by reacting with $Al(OH)_4^-$ and CO_3^{2-}.

The effect of synthesis pH on BET surface areas was also examined in Fig. 4(b). BET surface area first decreased from 192 m^2/g to 14.4 m^2/g with an increase in pH from 6.5 to 9. When pH was 6.5 or 7, the main product was amorphous AlOOH; therefore, it is easy to understand their relatively high surface areas (167–192 m^2/g). However, at synthesis pH of 8 or 9, the surface areas became very small (14.4–55.2 m^2/g). This might be due to the main products being MgAl–NO_3 and/or MgAl–HCO_3. As mentioned above, both NO_3^- and HCO_3^- anions will lead to HT having a very small surface area. The surface area increased sharply to 110 m^2/g at pH = 10; and further increasing pH to 14 slightly decreased the BET values. It was for the first time for us to observe that the synthesis pH value had a great effect on the pore size of synthesized Mg_3Al_1–CO_3 HTs. When pH was between 6 and 9, the average pore size kept constant at 3.7 nm. However, the average pore size gradually increased from 3.7 nm to 18.3 nm when the pH increased from 9 to 14 (not shown here). From these results, it can be concluded that the Mg/Al ratio, BET surface area, and pore size distribution of synthesized HTs can be tuned by changing synthesis pH values.

The CO_2 adsorption capacities of Mg_3Al_1–CO_3 HTs synthesized at pH ranging from 6.5 to 14 were then tested. Prior to each adsorption test, fresh HTs were first calcined at 400 °C in Ar for 5 h. The temperature profile for this test is shown as the inset of Fig. 5(a). The in situ pretreatment was performed at 400 °C under N_2 for 1 h, after which the sample was cooled down to adsorption temperature and held at that temperature for 0.5 h for the purpose of stabilization. The feed gas was then switched into CO_2 for adsorption. Fig. 5(a) indicates that the CO_2 adsorption capacity first increased with the increase of pH from 6.5/7 to 10. At pH 6.5 and 7, although the BET surface areas were very high (ca. 165–190 m^2/g, see Fig. 4), the Mg/Al ratio was too low to have sufficient Mg–O sites for CO_2 adsorption. Only a very small amount of CO_2, ca. 0.06–0.08 mmol/g was absorbed on these samples. The increase of Mg/Al ratio explains the increased of CO_2 adsorption capacity within the pH range of 6.5–10. Mg_3Al_1–CO_3 samples synthesized at pH 10–12 showed good performance for capturing CO_2, exhibiting an adsorption capacity of ca. 0.5 mmol/g. At pH 13 and 14, the CO_2 adsorption capacity was decreased to 0.36–0.39 mmol/g, which might be attributed to the decrease of surface area.

It is suggested that doping HTs with K_2CO_3 enhances CO_2 adsorption capacity [31–33]. Therefore, the promotion effect of K_2CO_3 was also studied by using Mg_3Al_1–CO_3 (pH = 10) as a representative HT. The CO_2 adsorption capacities of the doped HTs are shown in Fig. 5(b). By doping the HT with 20 wt.% of K_2CO_3, the CO_2 adsorption capacity was highly increased, achieving 0.81 mmol/g at 200 °C. Fig. 5(b) shows the adsorption temperature effect on the adsorption capacity of 20 wt.% K_2CO_3/Mg_3Al_1–CO_3 (pH = 10). It was found that the modified HTs had a very good CO_2 adsorption capacity at 300–350 °C, which is ideal for SEWGS reaction. The adsorption capacity reached 0.85 mmol/g at 300 °C. The long-term

stability of supported potassium is currently not clear to us and the relevant research is still undergoing. For many gas adsorption processes, steam generally has a negative effect on the performance of adsorbents, e.g., competing the adsorption sites. However, Ram Reddy et al. [13] proved that the presence of water in the feed enhances CO_2 sorption on HTs. Therefore, the CO_2 adsorption capacity of the synthesized 20 wt.% K_2CO_3/Mg_3Al_1–CO_3 (pH = 10) probably could be further increased when it runs in the presence of steam.

4. Conclusions

Although similar layered structure of HTs could be easily synthesized with various charge compensating anions including CO_3^{2-}, HCO_3^-, NO_3^-, SO_4^{2-}, and Cl^-, it was found that their physical as well as chemical properties are highly influenced by these anions. Using CO_3^{2-} as charge compensating anion, spheroidal "sand rose" type of HT was synthesized, showing a very high BET surface area of 114.3 m^2/g. However, with other anions, "stone" type HTs were formed, and their surface areas became very low (<9 m^2/g). In addition, the thermal stability of HTs was also influenced by anions, e.g. Mg_3Al_1–SO_4 showed relatively higher thermal stability than the others. Mg_3Al_1–CO_3 showed the highest CO_2 capture capacity of 0.53 mmol/g, which was much higher than those of other HTs with HCO_3^-, NO_3^-, SO_4^{2-}, and Cl^- anions (~0.2 mmol/g). The Mg_3Al_1–CO_3 was further studied using various synthesis pH values from 6.5 to 14. It was found that the Mg/Al ratio increased from 0.5 to 3.1 with an increase in pH from 6.5 to 10. Further increase in pH up to 14 has little effect on the Mg/Al ratio. The BET surface area and pore size distribution were also influenced by synthesis pH. The average pore size increased with increasing pH values. Mg_3Al_1–CO_3 synthesized at pH 10–12 showed the best performance for CO_2 capture at high temperature. By doping the Mg_3Al_1–CO_3 (pH = 10) with 20 wt.% K_2CO_3, the CO_2 adsorption capacity was increased to 0.85 mmol/g in the temperature range for WGS (300–400 °C).

Acknowledgements

This work is financially supported by the Thematic Strategic Research Program (Grant No. 0921380024) from the Agency for Science, Technology and Research (A*STAR) of Singapore. The authors would like to thank Dr. M.K. Schreyer for his assistance in XRD data analysis, Dr. P.K Wong and Keith Carpenter for their support of this project.

References

[1] B. Balasubramanian, A. Lopez Ortiz, S. Kaytakoglu, D.P. Harrison, Chem. Eng. Sci. 54 (1999) 3543.
[2] H.K. Rusten, E. Ochoa-Fernandez, H. Lindborg, D. Chen, H.A. Jakobsen, Ind. Eng. Chem. Res. 46 (2007) 8729.
[3] A.L. Ortiz, D.P. Harrison, Ind. Eng. Chem. Res. 40 (2001) 5102.
[4] H.Th.J. Reijers, S.E.A. Valster-Schiermeier, P.D. Cobden, R.W. van den Brink, Ind. Eng. Chem. Res. 45 (2006) 2522.
[5] K.B. Lee, M.G. Beaver, H.S. Caram, S. Sircar, J. Power Sources 176 (2008) 312.
[6] D.P. Harrison, Ind. Eng. Chem. Res. 47 (2008) 6486.
[7] P.D. Cobden, P. van Beurden, H.Th.J. Reijers, G.D. Elzinga, S.C.A. Kluiters, J.W. Dijkstra, D. Jansen, R.W. van den Brink, Int. J. Greenhouse Gas Control 1 (2007) 170.
[8] Z. Yong, A.E. Rodrigues, Energy Convers. Manage. 43 (2002) 1865.
[9] Q. Wang, J. Luo, Z. Zhong, A. Borgna, Energy Environ. Sci., in press, doi:10.1039/C0EE00064G.
[10] S. Choi, J.H. Drese, C.W. Jones, ChemSusChem 2 (2009) 796.
[11] W. Yang, Y. Kim, P.K.T. Liu, M. Sahimi, T.T. Tsotsis, Chem. Eng. Sci. 57 (2002) 2945.
[12] M.K. Ram Reddy, Z.P. Xu, G.Q. (Max) Lu, J.C. Diniz da Costa, Ind. Eng. Chem. Res. 45 (2006) 7504.
[13] M.K. Ram Reddy, Z.P. Xu, G.Q. (Max) Lu, J.C. Diniz da Costa, Ind. Eng. Chem. Res. 47 (2008) 2630.
[14] A.L. Mckenzie, C.T. Fishel, R.J. Davis, J. Catal. 138 (1992) 547.
[15] T. Horiuchi, H. Hidaka, T. Fukui, Y. Kubo, M. Horio, K. Suzuki, T. Mori, Appl. Catal. A: Gen. 167 (1998) 195.
[16] N.D. Hutson, B.C. Attwood, Adsorption 14 (2008) 781.
[17] Y. Lwin, F. Abdullah, J. Therm. Anal. Calorim. 97 (2009) 1572.
[18] X.P. Wang, J.J. Yu, J. Cheng, Z.P. Hao, Z.P. Xu, Environ. Sci. Technol. 42 (2008) 614.
[19] C.T. Yavuz, B.D. Shinall, A.V. Iretskii, M.G. White, T. Golden, M. Atilhan, P.C. Ford, G.D. Stucky, Chem. Mater. 21 (2009) 3473.
[20] Q. Wang, H.H. Tay, D.J.W. Ng, L. Chen, Y. Liu, J. Chang, Z. Zhong, J. Luo, A. Borgna, ChemSusChem 3 (2010) 965.
[21] T. López, P. Bosch, M. Asomoza, R. Gómez, E. Ramos, Mater. Lett. 31 (1997) 311.
[22] S. Miyata, Clay Miner. 23 (1975) 369.
[23] S. Miyata, A. Okada, Clay Miner. 25 (1977) 14.
[24] R.S. Zhai, A. Das, C.K. Hsu, C.C. Han, T. Canteenwala, L.Y. Chiang, T.J. Huang, Carbon 42 (2004) 395.
[25] H. Zeng, Z. Feng, X. Deng, Y. Li, Fuel 87 (2008) 3071.
[26] M.R. Othman, N.M. Rasid, W.J.N. Fernando, Chem. Eng. Sci. 61 (2006) 1555.
[27] M. Islam, R. Patel, J. Hazard. Mater. 169 (2009) 524.
[28] Z.P. Xu, G. Stevenson, C.Q. Lu, G.Q. Lu, J. Phys. Chem. B 110 (2006) 16923.
[29] F. Cavani, F. Trifirò, A. Vaccari, Catal. Today 11 (1991) 173.
[30] N.D. Hutson, S.A. Speakman, E.A. Payzant, Chem. Mater. 16 (2004) 4135.
[31] E.L.G. Oliveira, C.A. Grande, A.E. Rodrigues, Sep. Purif. Technol. 62 (2008) 137.
[32] K.B. Lee, A. Verdooren, H.S. Caram, S. Sircar, J. Colloid Interface Sci. 308 (2007) 30.
[33] S. Walspurger, L. Boels, P.D. Cobden, G.D. Elzinga, W.G. Haije, R.W. van den Brink, ChemSusChem 1 (2008) 643.